Supporting Information: Energy Landscape of the Charge Transfer Reaction at the Complex Li/SEI/Electrolyte Interface

Yunsong Li and Yue Qi*

[1]Department of Chemical Engineering and Materials Science, Michigan State University, East Lansing, MI 48824, USA

Computational Details of the SCC-DFTB and DFT Calculations

We employed SCC-DFTB calculations to evaluate the energy landscape at the electrode/SEI/electrolyte interface. All SCC-DFTB calculations were performed with the DFTB+ code [1]. All SCC-DFTB minimization calculations were performed after relaxing the structure with COMPASS II force field (Li-metal: li_m; Li^+ ion: li+; CO_3^{2-}: c3i and o1-; C=O: c3'' and o1=; $C_2H_4O_2$: c4o, h1, and o2s). When there were Li^+-ion dissolved in the electrolyte, the solvation shell structure formed during classical MD simulations became a key step to provide the initial structure for SCC-DFTB relaxation. During SCC-DFTB optimization, only atomic positions were relaxed until a maximum force component of 10^{-4} eV $Å^{-1}$ was achieved. The relaxed structure, especially the liquid phase, was subjected to SCC-DFTB molecular dynamics (MD) simulations with NVT ensemble at 450 K for 50 ps to obtain the average total energy (the summation of potential energy and kinetic energy). The Brillouin zone was sampled with a 2×2×1 mesh including the Γ point. The Lennard-Jones dispersion model was used to correct van der Waals interactions. To locate the electron, we have computed atomic charges based on the Mulliken population for an atomic-like basis.

We employed first-principles calculations to evaluate workfunction, solvation energy, and the electrochemical reaction at the electrode/SEI/electrolyte interface. All the first principles calculations were performed using plane-wave DFT implemented in the Vienna Ab initio Simulation Package (VASP) [2-4]. The exchange-correlation functional was treated in the spin-polarized Generalized Gradient Approximation (GGA) as parameterized by Perdew-Burke-Ernzerhof (PBE) with the projected augmented wave (PAW) method [5]. The standard version of the PAW potentials for Li, C, H and O supplied with VASP was used. Convergence with respect to both energy cutoff and the k-point mesh was tested. As a result of the convergence test, a plane wave cutoff of 600 eV was applied for all Li metal bulk, Li slab, and interface structures. A k-point

mesh of (11 × 11 × 11), (4 × 4 × 1) and (2 × 2 × 1) in the Monkhorst−Pack sampling scheme including the gamma point were used for bulk, slab, and interface structures, respectively. Spin polarization was taken into account and the Methfessel–Paxton method was employed to determine electron occupancies with a smearing width of 0.1 eV in all cases. The vdW (van der Waals)-DF exchange-correlation functional was used for interface structures. This particular exchange-correlation functional is capable of capturing van der Waals interactions, which play an important role in surface interaction. The convergence criterion for ionic relaxations was 10^{-6} eV per supercell and the Hellmann−Feynman force was converged to 0.01 eV $Å^{-1}$. The clean Li(001) surface was modeled by a slab consisting of ten Li atomic layers separated by the vacuum thickness of 15 Å.

Charge Transfer Reaction Energy Landscape

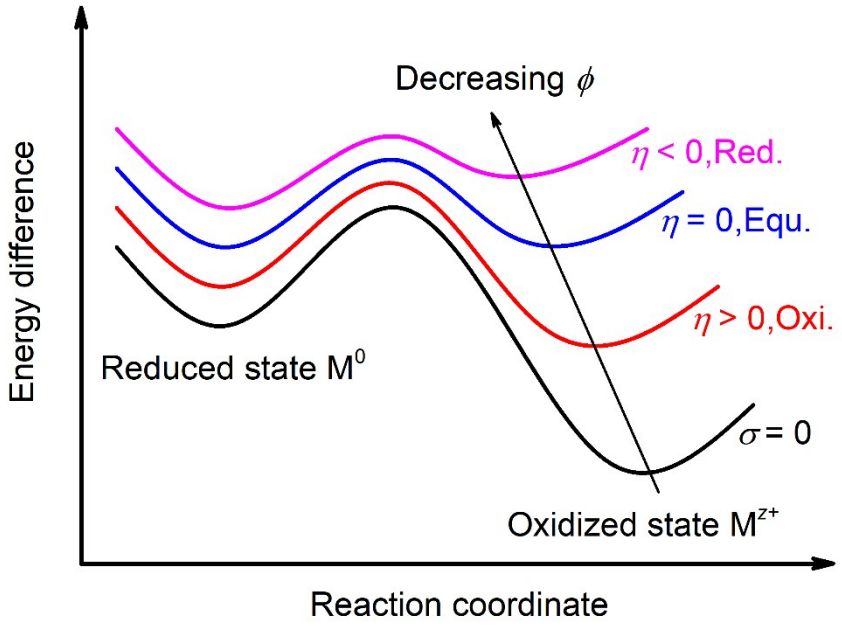

Fig S1 Illustrate the energy landscape along the reaction coordinate under different *Galvani* potential ϕ. The blue curve indicates the electrochemical equilibrium condition, noted as $\eta = 0$.

The Potentials Drop in the Explicit Interface Model

To evaluate the effects of the electric potential on Li metal surface, ϕ, on the electrochemical reaction energy landscape and to ensure the simulation cell is reasonable long enough, we estimated the electric potential distribution along the normal direction of the Li/Li_2CO_3/EC interface via classical electrical double layer (EDL) model. First, the electric potential drop through the Li_2CO_3 layer was estimated based on a charged plane sheet model with infinite size,

$$\phi(x) = 2\pi\sigma k x \text{ and } k = \frac{1}{4\pi\varepsilon_0\varepsilon_r} \quad \text{(S1)}$$

where σ is the charge density on the Li-metal electrode, x is the distance from the Li-metal surface, ε_0 and ε_r are the dielectric constants of vacuum and Li_2CO_3 relative to vacuum, and ε_r=4.9.[6] For the EC electrolyte, the Debye-Hückel double layer model was used to estimate the electric potential drop,

$$\frac{d^2\phi}{dx^2} = \kappa^2\phi, \text{ where } \kappa^2 = \frac{2\beta q^2 c_B}{\varepsilon_0\varepsilon_r} \quad \text{(S2)}$$

where x is the distance from the Li_2CO_3 surface, c_B is related to Li^+ ion concentration in the EC electrolyte, and ε_r are the dielectric constants of EC electrolyte with the value of 95.3.[7] The estimated electric potential distributions along the normal direction of the Li/Li2CO3/EC interface as a function of charge density on the Li-metal surface are shown in **Fig. S2a**. The electric potential dropped obviously through the SEI due to its insulating nature, and then dropped to zero quickly in liquid EC, as the highly polarized EC has a short Debye length.

We also directly computed the averaged electrostatic potential from DFT (**Fig. S2b**) for the reduced state with one Li^+ in the electrolyte. It indeed shows that the average potential is flat at the center of the electrolyte, i.e. the electric field is zero. The positive potential in the Li-metal slab in DFT is caused by Li tends to push electrons to the surface even in a neutral state. This has been observed in other DFT calculations [8]. This also causes a large negative potential in Li_2CO_3, as shown in Fig S2b. Nevertheless, both the DFT and continuum model showed zero potential at the center of the liquid electrolyte, indicating the liquid is out of the Helmholtz layer on the charged Li-surface.

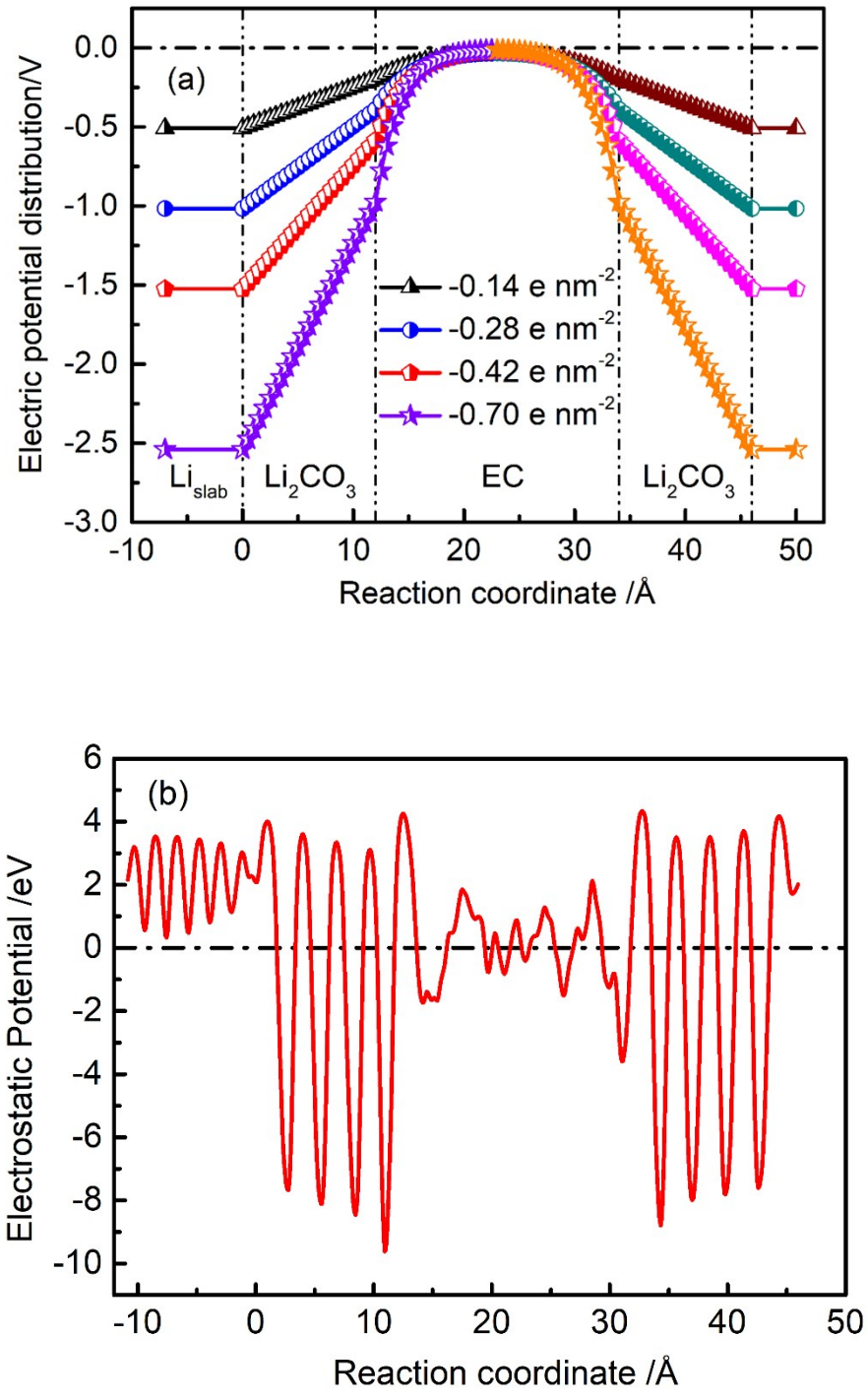

Fig. S2. (a) The electric potential distribution as a function of charge density in the simulation cell via classical models. (b) Calculated electrostatic energy profile in $Li/Li_2CO_3/EC$ interface by DFT.

Thermodynamics Cycle for the Charge Transfer Reaction

The charge transfer reaction in **Eq 1** can be rewritten to include the insulating effect of the SEI layer, assuming Li^+ ion dissolved in the EC solvents.

$$Li_{n-1}(metal, with\ V_{Li}) + Li^+(EC)_m + e^-(on\ Li\ metal) \xrightarrow{\Delta G^0} Li_n(metal) + (EC)_m \quad \text{(S3)}$$

One can compute or measure each energy term in the thermodynamic cycle illustrated in **Fig. S3** as the following:

$$\Delta G^0 = -E_f(V_{Li}) - E_{vap} - E_{ion} + W_f + E_{sol}(Li^+) \quad \text{(S4)}$$

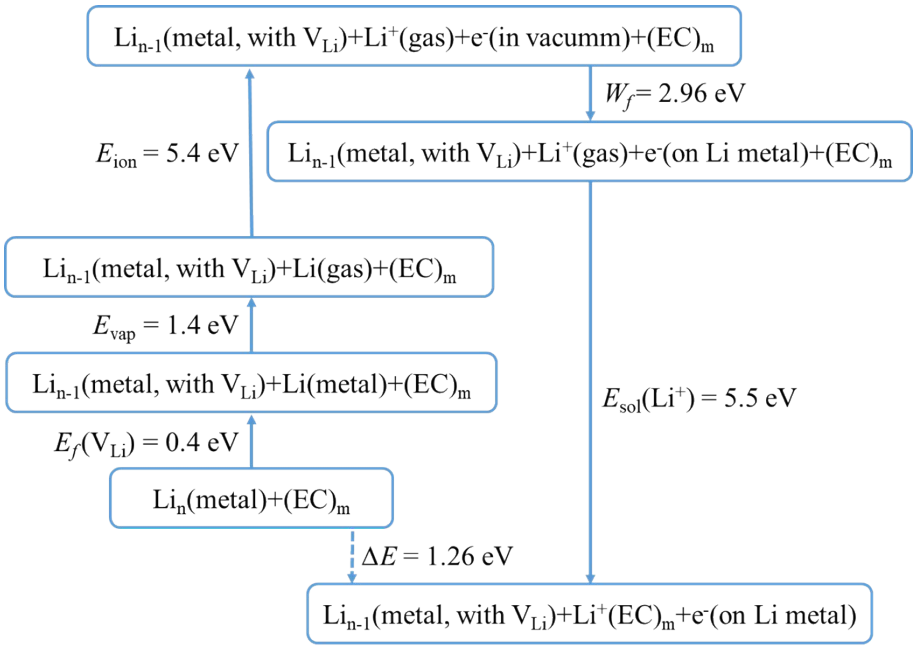

Fig. S3. Thermodynamics cycle of charge transfer reaction.

The Effect of Li^+ Ion Concentration on Activity

The Li^+ ion activity in the electrolyte, a_{Li^+}, is the chemical potential difference between a real solution with respect to an ideal solution. Here it is linked to the solution energy change due to Li^+ ion concentration variation near the charged surface.

$$RTlna_{Li^+} = \mu_{Li^+} - \mu^0_{Li^+} \sim \Delta E_{sol}(Li^+) \quad \text{(S5)}$$

In order to explore the effect of Li^+ ion concentration on charge transfer reaction, SCC-DFTB MD simulations (with NVT ensemble at 450 K) was used to predicate the Li^+ ion average solvation energies (per Li^+) in EC-electrolyte with a set of bulk models including 32 EC liquid molecules and *n* (*n*=1-5) Li^+ ions. In order to verify the SCC-DFTB results, the relaxed bulk structures including 1 and 2 Li^+ ions after SCC-DFTB optimization were further used to compute the solvation energies with DFT (GGA/PBE) method. The calculated solvation energies as a function of Li^+ ion concentration in the electrolyte are shown in **Fig. S4**. It decreases slightly with increasing of Li^+ ion concentration.

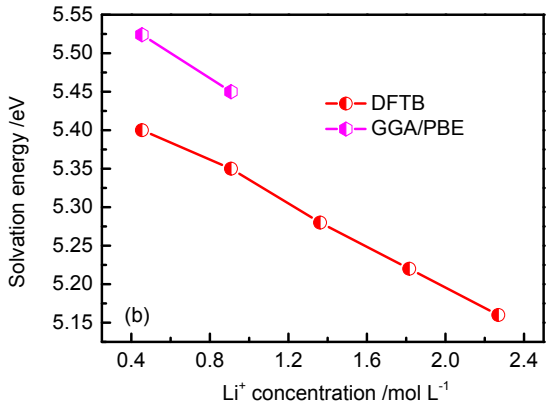

Fig. S4 Li^+ ion solvation energy with Li^+ ion concentration in the EC-electrolyte from DFT (GGA/PBE) and SCC-DFTB.

Table S1 The angle between the C=O bond direction and the normal of the Li_2CO_3/EC-electrolyte interface for Layer 1, 2, and 3 are 4 Å thick regions in parallel to the Li_2CO_3 surface, arranged in the sequence from closer to far away from the surface.

Charge density /e nm^{-2}	Average angle /°		
	1L	2L	3L
0	98.1±52.5	87.0±54.9	93.7±49.5
0.14	69.5±47.4	75.1±50.4	85.1±51.6
0.28	50.1±32.5	70.2±50.1	87.5±50.5

0.42	22.4±19.1	67.6±51.9	89.4±62.5
0.70	6.2±8.0	54.9±43.5	86.9±47.0

References

1. B. Aradi, B. Hourahine and T. Frauenheim, *J. Phys. Chem. A*, 2007, **111**, 5678-5684.
2. G. Kresse and J. Furthmüller, *Phys. Rev. B*, 1996, **54**, 11169-11186.
3. G. Kresse and J. Furthmuller, *Comput. Mater. Sci.*, 1996, **6**, 15-50.
4. G. Kresse and D. Joubert, *Phys. Rev. B*, 1999, **59**, 1758-1775.
5. P. E. Blöchl, *Phys. Rev. B*, 1994, **50**, 17953-17979.
6. K. F. Young and H. P. R. Frederikse, *J. Phys. Chem. Ref. Data*, 1973, **2**, 313-410.
7. D. S. Hall, J. Self and J. R. Dahn, *J. Phys. Chem. C*, 2015, **119**, 22322-22330.
8. K. Leung and C. M. Tenney, *J. Phys. Chem. C*, 2013, **117**, 24224-24235.